

Full Article

Cell and nucleus refractive-index mapping by interferometric phase microscopy and rapid confocal fluorescence microscopy

Shir Cohen Maslaton, Itay Barnea, Almog Taieb, and Natan T. Shaked*

Department of Biomedical Engineering, Faculty of Engineering

Tel Aviv University, Tel Aviv, Israel

***Correspondence:**

Natan T. Shaked

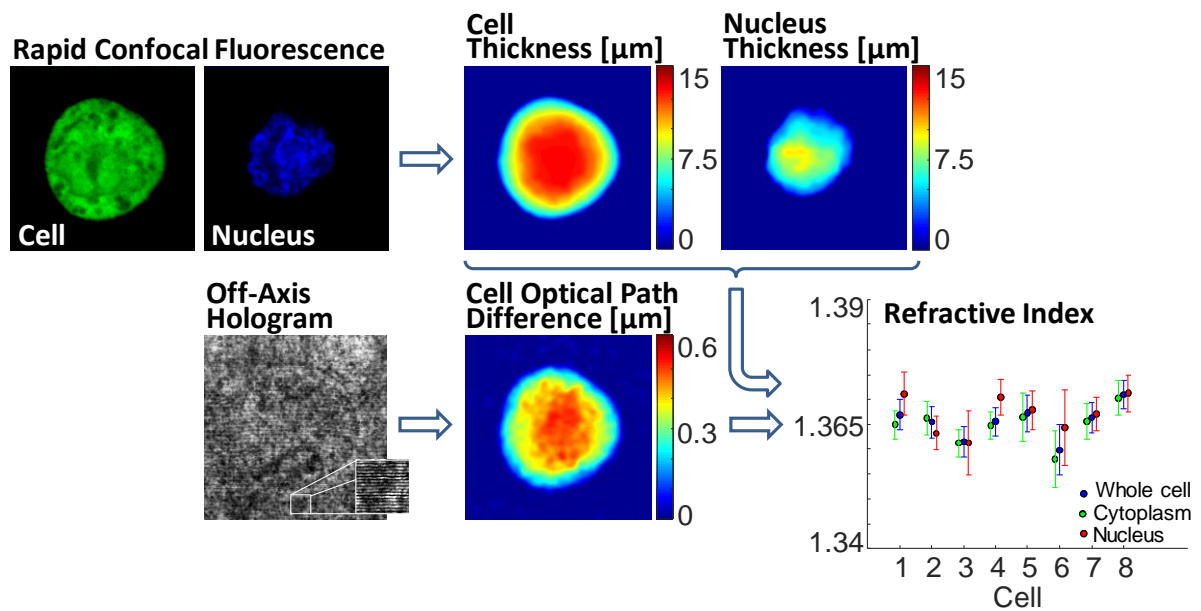
E-mail: nshaked@tau.ac.il

KEYWORDS: Cell imaging; Confocal fluorescence microscopy; Holographic microscopy; Quantitative phase imaging

Abstract

We present a multi-modal technique for measuring the integral refractive index and the thickness of biological cells and their organelles by integrating interferometric phase microscopy and rapid confocal fluorescence microscopy. First, the actual thickness maps of cellular compartments are reconstructed using the confocal fluorescent sections, and then the optical path difference map of the same cell is reconstructed using interferometric phase microscopy. Based on the co-registered data, the integral refractive index maps of the cell and its organelles are calculated. This technique enables rapidly measuring refractive index of live, dynamic cells, where interferometric phase microscopy provides quantitative imaging capabilities and confocal fluorescence microscopy provides molecular specificity of specific organelles. We acquire human colorectal adenocarcinoma cells and show that the integral refractive index values are similar for the whole cell, the cytoplasm and the nucleus on the population level, but significantly different on the single cell level.

Abstract Figure



Abbreviations: **RI**, refractive index; **IPM**, interferometric phase microscopy; **OPD**, optical path difference; **TPM**, tomographic phase microscopy; **SDCM**, Spinning-disk confocal microscopy; **HT29-GFP**, human colorectal adenocarcinoma; **GFP**, green fluorescent protein; **DMEM**, Dulbecco's modified Eagle's medium; **FBS**, fetal bovine serum; **FOV**, field of view; **BFM**, bright-field microscopy; **CoC**, coefficient of correlation; **SSIM**, structural similarity index

1. INTRODUCTION

Quantification and characterization of the refractive index (RI) of biological cells have great importance for both medical diagnosis and biological research. Such knowledge allows estimation of cellular protein concentration [1], hematologic diagnosis [2], quantification of cellular differentiation [3], identification of cells infection by pathogens [4], discrimination of lymphocyte cell types [5], and selection of sperm cells for in vitro fertilization [6]. Knowledge of the subcellular RI distribution, such as the nuclear and the cytoplasmic RIs, is also important for various biological assays such as cancer diagnosis by measuring the nuclear RI [7], and detection of alterations in DNA content through the cell cycle by measuring the nuclear RI [8].

Off-axis interferometric phase microscopy (IPM) is a quantitative phase imaging technique that enables high-contrast label-free imaging of live cells in vitro, without scanning and by one acquisition [9, 10]. This technique is based on digital off-axis holographic microscopy: it measures how much a light wave is delayed when passing through a sample in relation to a reference wave, while the two waves are projected at a small angle between them onto a camera that captures their interference pattern. Using IPM, the quantitative phase at each spatial location on a sample can be measured. This phase map is proportional to the optical path difference (OPD) of the sample relative to the surrounding medium. The OPD is equal to the sample thickness multiplied by the difference between the integral RI of the sample across the sample thickness and the surrounding medium RI. Therefore, IPM provides quantitative information about both the actual thickness and the integral RI of the sample, in a coupled manner. In order to use IPM for extracting the integral RI of a sample in one acquisition, prior measurement of the physical thickness of the sample is required.

Several methods have been previously suggested for solving this RI-thickness coupling problem for the cell as a whole. Such methods include performing two phase measurements while changing the RI of the surrounding medium, either via physical change of the medium

[11, 12], e.g. in a flow chamber, or via change of the illumination wavelength in a dispersive medium [13–15]. This approach allows obtaining, for each spatial location on the sample, two linear equations with two unknowns: the thickness and the integral RI. In this approach, suitable biocompatible medium supplemented materials that do not change the medium osmolarity are needed. Other methods include evaluating the sample thickness at each spatial location in addition to the IPM measurement, which allows the calculation of the integral RI at each location. Thickness evaluation can be achieved by assuming spherical [4, 16–22] or ellipsoidal [23] shape for cells in suspension. An alternative approach is physically measuring the cell thickness using atomic force microscopy [24, 25], confocal fluorescence microscopy [26], confocal reflectance microscopy [1], or by constraining cells into a microstructure with known dimensions [19]. Another approach for obtaining the RI and the cell morphology separately is tomographic phase microscopy (TPM). TPM can obtain the three-dimensional (3D) RI distribution of a cell, not just the integral of the RI across the cell thickness [27–32]. This can be achieved by capturing phase images of a sample from multiple angles and digitally processing them to create a 3D RI distribution. Due to the different perspectives required, either the sample or the illumination needs to be rotated. This approach is more complicated to implement than regular IPM and is limited to samples with dynamics slower than the angular acquisition rate.

In contrast to methods that allow the acquisition of the whole cell integral RI, without access to the cell organelles, other methods have evaluated the nucleus RI. For that purpose, nucleus thickness evaluation was done by actual isolation of the nucleus and then evaluation of its thickness by assuming a spherical shape [33, 34], or by fluorescent labeling of the nucleus inside the cell and then estimation of the nucleus thickness by assuming an ellipsoidal shape [23]. Nucleus thickness evaluation was also done by using a confocal fluorescence microscope, while labeling the whole cell and assuming negligible cytoplasmic thickness at a single estimated nucleus location [26], or by using a confocal reflectance microscope in order

to detect the contour of the nucleus inside the cell [1]. Nucleus RI evaluation was also performed by TPM combined with fluorescence for nucleus segmentation purposes [35, 36]. Some previous studies have reported that the nuclear RI is greater than that of the cytoplasm [28, 29, 35], whereas other studies have reported the contrary [23, 33, 34, 36], and only a few reported similarity between the two [26, 31].

Spinning-disk confocal microscopy (SDCM) [37, 38] enables rapid 3D imaging of fluorescently labeled biological specimens. Using this modality, thickness maps of specific fluorescent labeled cellular and subcellular structures, such as the cell nucleus, can be reconstructed [26]. In contrast to IPM, SDCM can provide molecular specificity of the cell organelles in 3D. However, it does not provide a quantitative measurement of the cell RI.

In this study, we present a new technique for decoupling both the integral RI and the thickness of biological cells as a whole and their nucleus and cytoplasm. This is done by incorporating IPM with SDCM. Sections of two fluorescently labeled cell components, the entire cell and the nucleus, were acquired using a SDCM, while cell off-axis hologram was acquired using IPM. The thickness maps of the whole cell, the cytoplasm and the nucleus were reconstructed from the fluorescent confocal sections, whereas the OPD map was reconstructed from the hologram. Then, the integral RI maps were calculated for the whole cell, the cytoplasm and the nucleus. This new technique enables RI-thickness decoupling of living cells that can be either in suspension or attached to the surface, can be dynamic and can undergo biological processes. Also, there is no need for nuclei isolation, or to transfer the cells between two different microscopes.

2. MATERIALS AND METHODS

2.1 Cell Culture and Sample Preparation

HT29-GFP (human colorectal adenocarcinoma) cell line was imaged by both IPM and SDCM. The green fluorescent protein (GFP) gene was previously transfected into the cells using adenovirus vector [39]. HT29-GFP clones were examined by flow cytometry and the clone with the highest GFP expression level was used in this study for imaging. The cells were grown in high-glucose Dulbecco's modified Eagle's medium (DMEM), supplemented with 10% heat-inactivated fetal bovine serum (FBS) and 1% penicillin-streptomycin (Biological Industries, Beit HaEmeq, Israel). Cells were incubated under standard conditions at 37 °C and 5% CO₂. Prior to imaging, cells were harvested using a trypsin solution, and then centrifuged at 400g for 5 min. The supernatant was removed and the pellet was resuspended in PBS (1 ml) supplemented with EDTA (1mM). The PBS-EDTA solution had a RI of 1.3342 ± 0.0003 , as measured using a refractometer (PAL-RI, 3850, Atago, Tokyo, Japan). For nucleus fluorescent labeling, the cells were stained with 10 µg/ml Hoechst 33342 dye (Sigma-Aldrich, St. Louis, MO, USA) and incubated in the dark for 30 min. Then, the cells were inserted into a customized imaging chamber, made out of glass coverslips that were glued together with wax, creating a spacer of approximately 0.16 mm.

As test targets, we also measured fluorescent microbeads, 6 µm in diameter, based on melamine resin, FITC-marked, with RI of 1.68 (Fluka Analytical, Sigma-Aldrich, St. Louis, MO, USA). The raw solution was diluted 100 times and then dried onto a coverslip. We used oil immersion medium with RI of 1.518 (Olympus, Tokyo, Japan) as the surrounding medium, to create reasonable RI mismatch.

2.2 Optical Setup

The imaging system, shown in Fig. 1, was composed of a commercial inverted microscope (IX83, Olympus, Tokyo, Japan), which contained an epi-illumination spinning-disk confocal

imaging unit (CSU-X1, Yokogawa, Tokyo, Japan), and a custom-built external interferometric module, which was integrated at the commercial microscope output.

For holographic imaging, a low-temporal-coherence laser light with a central wavelength of 690 ± 3 nm was generated by supercontinuum laser source SC (S422-205-000, SuperK Extreme, NKT, Birkerød, Denmark), coupled to acousto-optic tunable filter AOTF (A901-100-000, SuperK SELECT, NKT, Birkerød, Denmark). The light beam was reflected by mirror M1 and entered the commercial microscope. Inside the microscope, the beam passed through the sample S, and was magnified by microscope objective MO (UPlanSApo, 100 \times , 1.4 NA, oil-immersion, Olympus, Tokyo, Japan). The beam was reflected out of the commercial microscope using beam splitter BS1, located in the microscope infinity space, and passed through tube lens TL1 ($f=200$ mm). Then, the beam passed through lens L1 ($f=100$ mm), which was the first lens of a 4f lens configuration, and entered the external off-axis flipping interferometric module [40]. In this module, the beam was split by beam splitter BS2. One beam was reflected back from slightly tilted mirror M2, and the other beam was reflected back from retro-reflector RR, which flipped the optical field of view (FOV) of that beam. Then, the two beams reunited at BS2 and passed through lens L2 ($f=100$ mm), the second lens of the 4f lens configuration. The two beams were projected onto digital camera C1 (DCC1545M, 1.3 Megapixels 1280 \times 1024, square pixels of 5.2 μ m, Thorlabs, Newton, New Jersey, USA) with a small off-axis angle between them. This created an off-axis image hologram on the camera. By making sure that one half of the sample optical FOV is empty, this half could be considered as the reference beam.

For confocal imaging, fluorescence excitation laser light was generated by multi-line laser source LC (VS-Laser control, Visitron Systems, Puchheim, Germany), which included two lasers: central wavelength of 488 nm for GFP excitation and central wavelength of 405 nm for Hoechst excitation. The excitation light alternated between the two wavelengths for each scanned axial plane in order to obtain fluorescent signal from both the whole cell and the

nucleus almost simultaneously. The spinning-disk SD in the excitation light path was composed of an array of microlenses that formed many excitation light spots, and a pinholes array arranged to match each focal point of the microlenses array. This enabled simultaneous illumination of many light spots on the sample in parallel. Dichroic mirror DM was placed inside the SD, which permitted passing of the excitation light and reflectance of the fluorescence emission. The fluorescently labeled sample then emitted green light from the entire GFP-modified-cell, and blue light from the Hoechst-labeled nucleus. The light emitted from the sample was magnified by MO and transmitted by BS1 back to the SD and to the DM, which reflected the light toward tube lens TL2. Then, the beam was projected onto camera C2 (acA2440-75um, 5 Megapixels 2448×2048, square pixels of 3.45 μm , Basler, Ahrensburg, Germany), which captured the spatial distribution of the fluorescent signal. Using SDCM, a series of sections images along the z-axis were acquired with objective increments of 0.1 μm and 0.5 μm for the fluorescent beads and the HT29-GFP cells, respectively. The theoretical maximum acquisition speed of the SDCM is 2000 frames per second. On average, 72 sections were needed for acquiring both the nucleus and the whole cell fluorescent sections for each cell, meaning that on average 0.036 sec were required for obtaining the confocal fluorescent signal of each cell. However, in our experiment in order to obtain high contrast images, we set the exposure time to 0.2 sec per each section, resulting in 14.4 sec for imaging all sections in a cell. This exposure time could have potentially been reduced by increasing the fluorescent signal, for example, by using higher dyes concentration or more stable fluorescent dyes or by reducing the number of sections. This combined IPM / SDCM imaging system allowed us to obtain cell holograms and fluorescent confocal sections images without moving the sample.

2.3 Image Processing

2.3.1 OPD Reconstruction

Digital reconstruction of the sample OPD from the captured hologram was performed using the off-axis Fourier-based algorithm [41] using a MATLAB software. This algorithm includes two-dimensional (2D) Fourier transform of the off-axis sample hologram, followed by cropping of one of the cross-correlation terms and performing a 2D inverse Fourier transform. The argument of the resulting matrix is the sample wrapped phase. In order to compensate for beam curvatures and stationary aberrations in the beam profile, we subtracted from the sample wrapped phase the wrapped phase extracted from a hologram that was captured without any sample. Then, we applied the unweighted least squares phase unwrapping algorithm [42] to resolve the 2π phase ambiguities. The resulting unwrapped quantitative phase map was multiplied by the wavelength and divided by 2π in order to obtain the OPD map of the sample. Note that we acquired image holograms; thus the camera is positioned in the image plane of the sample. Since we used an external interferometer, where the reference beam is created after passing through the sample, our background value was zero, as required, and we did not need to compensate for the optical path difference between the sample and the reference beams, resulting from the propagation in the immersion oil and the glass of the coverslips.

2.3.2 Thickness Calculation

In order to calculate the thickness map from the fluorescence sections acquired by the SDCM, each section was binarized using imageJ software, where pixels that contained sample information were set to 1 and background pixels were set to 0. Then, all of the binarized sections were accumulated, to obtain the 2D unscaled thickness map of the sample, and the result was multiplied by the z-axis increment to obtain the thickness image of the sample.

Due to the RI mismatch between the immersion oil and the surrounding medium, the movement of the focal plane in the sample did not necessarily follow the movement of the objective when acquiring z sections through the sample. Therefore, scaling was needed [43].

We have chosen an empirical method in order to find the scaling factor. Using the SDCM, we imaged four fluorescent beads that had known dimensions, in the same medium in which the cells were imaged. We then calculated these fluorescent beads axial diameter using the objective z-axis increments and found the scaling factor by dividing the actual diameter of the beads by their calculated diameter. The thickness images of the cells, calculated from fluorescent sections acquired by SDCM, were scaled by this factor that was found by analyzing the beads as explained above.

2.3.3 Image Registration

The thickness and the OPD images were reconstructed from images taken using two different cameras. Therefore, image registration was needed. For registration purposes, we imaged 1951 US Air Force (USAF) resolution target both by IPM and bright-field microscopy (BFM), which was also supported by the commercial microscope and used the same camera as the confocal modality. The stages of the image registration included resizing the BFM image to the same size of the IPM image, then calculating the coefficient of correlation (CoC) between the two images [44, 45] for different rotating angles and cropping in each direction. The CoC was calculated after rotating, cropping, resizing again and color intensity normalization. The rotating angle and the cropping that resulted in the highest CoC was chosen as the registration transformation.

2.4 RI-Thickness Decoupling Theory

The reconstructed OPD at each pixel can be written as [23]:

$$OPD(x, y) = (n_{cell}(x, y) - n_0) \cdot h_{cell}(x, y), \quad (1)$$

where $n_{cell}(x, y)$ is the whole cell integral RI at each pixel, n_0 is the surrounding medium RI, and $h_{cell}(x, y)$ is the whole cell thickness at each pixel. Therefore, the whole cell integral RI at each pixel can be calculated by:

$$n_{cell}(x, y) = \frac{OPD(x, y)}{h_{cell}(x, y)} + n_0. \quad (2)$$

The whole cell weighted average RI for the entire cell can be calculated by weighting all calculated whole cell integral RI values at each pixel with the corresponding thickness at that pixel as follows [18, 34]:

$$\bar{n}_{cell} = \frac{\sum_{x, y} n_{cell}(x, y) \cdot h_{cell}(x, y)}{\sum_{x, y} h_{cell}(x, y)}. \quad (3)$$

The nucleus location can be identified by combining quantitative phase imaging and fluorescence microscopy (i.e., [46]). Assuming that the cell is composed of a cytoplasm and a nucleus, the OPD can be written as follows:

$$OPD(x, y) = (n_{cyt}(x, y) - n_0) \cdot h_{cyt}(x, y) + (n_{nuc}(x, y) - n_0) \cdot h_{nuc}(x, y), \quad (4)$$

where $n_{cyt}(x, y)$ and $n_{nuc}(x, y)$ are the cytoplasm and nucleus integral RI at each pixel, respectively, and $h_{cyt}(x, y)$ and $h_{nuc}(x, y)$ are the cytoplasm and nucleus thickness at each pixel, respectively. For pixels that contain only cytoplasm contribution, the equation can be reduced to:

$$OPD(x, y) = (n_{cyt}(x, y) - n_0) \cdot h_{cyt}(x, y), \quad \forall (x, y) \in cytoplasm. \quad (5)$$

Therefore, the cytoplasm integral RI at each pixel can be calculated by:

$$n_{cyt}(x, y) = \frac{OPD(x, y)}{h_{cyt}(x, y)} + n_0, \quad \forall (x, y) \in cytoplasm. \quad (6)$$

The cytoplasm weighted average RI for the entire cell can be calculated by:

$$\bar{n}_{cyt} = \frac{\sum_{x, y} n_{cyt}(x, y) \cdot h_{cyt}(x, y)}{\sum_{x, y} h_{cyt}(x, y)}, \quad \forall (x, y) \in cytoplasm. \quad (7)$$

Assuming that the RI of the cytoplasm is homogenous, the cytoplasm weighted average RI value can be substituted in Eq. 4 in order to estimate the nucleus integral RI at each pixel:

$$n_{nuc}(x, y) = \frac{OPD(x, y) - (\bar{n}_{cyt} - n_0) \cdot h_{cyt}(x, y)}{h_{nuc}(x, y)} + n_0, \quad \forall (x, y) \in nucleus. \quad (8)$$

The nucleus weighted average RI for the entire cell can be calculated by:

$$\bar{n}_{nuc} = \frac{\sum_{x, y} n_{nuc}(x, y) \cdot h_{nuc}(x, y)}{\sum_{x, y} h_{nuc}(x, y)}, \quad \forall (x, y) \in nucleus. \quad (9)$$

3. RESULTS

3.1 Validation of the Decoupling Method

In order to validate the decoupling method, ten fluorescent beads with a known RI and dimensions were imaged, and their weighted average RI and thickness were calculated. Representative images of the analysis done on one of the beads are shown in Fig. 2. Figure 2(a) shows the off-axis hologram acquired by IPM, and Fig. 2(b) shows the extracted OPD image. Figure 2(c) shows the measured thickness profile obtained based on imaging the fluorescent bead in 3D using the SDCM. Figure 2(d) shows the theoretical thickness map of the bead, as obtained by assuming a perfect sphere. The CoC and the structural similarity index (SSIM) [44] between the images were 0.9827 ± 0.0083 and 0.8731 ± 0.0258 , respectively, showing an excellent match between the theoretical thickness and the calculated one. Figure 2(e) shows the calculated integral RI map (obtained using the measured thickness map shown in Fig. 2(c), the OPD map shown in Fig. 2(b), and Eq. 2), which appears homogeneous, as expected. The RI of all of the beads was 1.6779 ± 0.0041 .

3.2 Measurement of RI in Cells

We measured OPD profiles of 54 HT29-GFP cells. The cells were imaged using both IPM and a 2D (not confocal) fluorescence microscopy, which was also supported by the commercial microscope [23]. The fluorescent signal was recorded in order to obtain 2D segmentation of the cell organelles in the OPD profiles. Results of the averaged OPD values of various cell components are presented in Fig. 3. Figure 3(a) shows the averaged OPD values of the whole cell, cytoplasm and nucleus for each cell. Although it seems that the range of the possible OPD values among different cells is very large, for each cell, in 94.4% of the cases, the averaged OPD value of the cytoplasm was the lowest and the averaged OPD value of the nucleus was the highest. A possible reason for higher OPD values in the nucleus area per cell might be due to the fact that in most of the HT29-GFP cells, the nucleus is located at

the center of the cell, where the thickness is the highest. Figure 3(b) shows the averaged OPD values of the whole cell, the cytoplasm and the nucleus for group of cells. The OPD values of the whole cell, the cytoplasm and the nucleus were 0.3217 ± 0.0988 , 0.2636 ± 0.0864 and 0.3780 ± 0.1156 , respectively. The p values of the whole cell and the cytoplasm groups, the whole cell and the nucleus groups, and the cytoplasm and the nucleus groups were 0.0015, 0.0076 and $7.1375 \cdot 10^{-8}$, respectively, indicating statistical significance.

The first eight HT29-GFP cells from Fig. 3(a) were imaged also using SDCM with two different staining agents for obtaining separate fluorescent sections of the whole cell and the nucleus. These sections were analyzed to extract separate thickness images of the whole cell, the nucleus and the cytoplasm. Figure 4 shows images obtained by the combined IPM / SDCM imaging system for one representative cell. Figure 4(a) shows the BFM image, Fig. 4(b) shows the off-axis hologram, and Figs. 4(c) and (d) show the middle sections of the confocal fluorescent signal of the whole cell and the nucleus, respectively. This study was conducted on single cells in suspension; however, it could easily be performed on cells that are attached to the surface, or cells in a more confluent culture, and therefore exhibit a non-spherical shape. Due to the fact that the thickness evaluation in this methods do not rely on any previous assumption on the morphology of the analyzed cells, other types of shapes should not have any impact on the results. Figure 4(e) shows the full 3D image of the cell reconstructed from all confocal fluorescent sections of the whole cell and the nucleus. Even though the cells were in suspension, most of the cell nuclei do not show a distinctly spherical or ellipsoidal shape, which experimentally demonstrates our ability to deal with non-round shapes. Therefore, calculating the thickness using a confocal microscope is more accurate than assuming spherical or ellipsoid shape for them, as was previously performed [23, 33, 34].

Figure 5 shows the processing stages and the resultant integral RI maps of the same representative cell presented in Fig 4. Figure 5(a) shows the OPD map extracted from the acquired hologram. Figures 5(b), (c) and (d) show the thickness maps of the whole cell, the

nucleus and the cytoplasm, respectively, calculated from the confocal fluorescent sections. Figures 5(e), (f) and (g) show the calculated integral RI maps of the whole cell, the nucleus and the cytoplasm, calculated using Eqs. 2, 8 and 6, respectively, by utilizing the combined data obtained from IPM and SDCM. A relatively uniform integral RI can be seen throughout the whole cell without significantly different values for the location of the nucleus and the cytoplasm. Therefore, we conclude that the nucleus location cannot be accurately determined from the whole cell integral RI map.

Figure 6 shows the extracted weighted average RI of the whole cell, the cytoplasm and the nucleus, calculated using Eqs. 3, 7 and 9, respectively. Figure 6(a) shows the weighted average RI and the STD of the whole cell, the cytoplasm and the nucleus for each cell. For most cells, the calculated weighted average RI of the nucleus was slightly higher than that of the cytoplasm. In one cell, the nucleus weighted average RI was lower than that of the cytoplasm, and in another cell the two RIs were similar. In these two cells, the average OPD of the nucleus was higher than that of the cytoplasm, as for all of these eight cells. Figure 6(b) shows the weighted average RI values of the whole cell, the cytoplasm and the nucleus for groups of cells, resulted in values of 1.3655 ± 0.0035 , 1.3647 ± 0.0037 and 1.3670 ± 0.0038 , respectively. We can see that RI of the whole cell, the cytoplasm and the nucleus are very similar, while the nucleus mean RI is slightly higher than that of the cytoplasm. The p values of the whole cell and the cytoplasm groups, the whole cell and the nucleus groups, and the cytoplasm and the nucleus groups were 0.6661, 0.3988 and 0.2256, respectively, which indicates statistical insignificance. We assume that the low concentration of the fluorescent dyes inside the cells does not affect the cells RI. This is also supported by Ref. [36], in which cells RI values were obtained using fluorescent staining and were then validated using a label free method.

Figure 7 shows BF images of many HT29-GFP cells, to demonstrate the low intracellular contrast, which supports the findings presented in Fig. 6, indicating no significant differences between the RI of the whole cell, the cytoplasm and the nucleus.

4. DISCUSSION AND CONCLUSIONS

RI of biological cells is one of the key biophysical parameters with potential medical value. From the analysis of a group of HT29-GFP cells, we found that the mean RI values of the whole cell, the cytoplasm and the nucleus are very similar, with mean nucleus RI slightly higher than that of the cytoplasm. Additionally, we found that for some cells, the nucleus weighted average RI is higher than that of the cytoplasm and for others it is lower, but in most of the cases the nucleus weighted average RI is higher. This could be explained by the fact that each cell was at different stage in the cell cycle, which results in different nucleus RI [8], or by the fact that each nucleus contained different amount and size of nucleoli, which contribute to the high RI of the nucleus [1, 27, 30, 31, 36], or due to different cell size [17]. For each cell, high RI around the nucleus may correspond to the presence of rough endoplasmic reticulum [31].

The range of RI values obtained for the HT29-GFP cells corresponds to those reported in the literature for the same type of cell [29, 32]. In those publications, the cell nucleoli and nuclear periphery also demonstrated higher RI than the mean RI of the cytoplasm, which is compatible with our findings. In addition, the RI range that we obtained also resembles to those reported in the literature for other types of cancer cells [1, 16, 17, 19, 30, 31].

In this study, we presented a new technique for decoupling the integral RI and the thickness of biological cellular compartments by incorporating IPM with rapid confocal fluorescence microscopy, in a way that provides quantitative morphological imaging with molecular specificity, even for the cell nucleus. Thus, the two incorporated modalities are complementary to each other and allow quantitative investigation of subcellular structures. This method can be applied for living cells characterized by non-spherical shapes. Our

technique is based on imaging by two cameras at the same time; therefore, there is no need for moving the sample between different microscopes. We calculated the RI for cells in suspension, but our method can be applied to cells in the adherent state as well, which may exhibit different RI [4]. In addition, different cellular compartments, such as the nucleoli and mitochondria, can be fluorescently labeled and their RIs can be calculated as well using this method. Fully automated measurements could be possible by using flow chambers combined with optical tweezers to trap cells while being imaged and GPU-based rapid processing.

ACKNOWLEDGMENTS

This research was funded by Horizon 2020 European Research Council (ERC) Grant No. 678316. We thank Prof. Nadir Arber from the Laboratory of Molecular Biology at Tel Aviv University for generously providing us the HT29-GFP cell line.

AUTHOR CONTRIBUTIONS

S.C-M. and N.T.S. were involved in conceptualization, investigation, and writing the original draft. I.B. was involved in investigation and writing, and A.T. was involved in investigation. N.T.S. supervised the project.

CONFLICT OF INTEREST

The authors declare no financial or commercial conflict of interest.

REFERENCES

- [1] N. Lue, W. Choi, G. Popescu, Z. Yaqoob, K. Badizadegan, R. R. Dasari and M. S. Feld, *J. Phys. Chem. A*, 2009, *113*, 13327.
- [2] G. Mazarevica, T. Freivalds and A. Jurka, *J. Biomed. Opt.*, 2002, *7*, 244.
- [3] K. J. Chalut, A. E. Ekpenyong, W. L. Clegg, I. C. Melhuish and J. Guck, *Integr. Biol.*,

- 2012, 4, 280.
- [4] A. E. Ekpenyong, S. M. Man, S. Achouri, C. E. Bryant, J. Guck and K. J. Chalut, *J. Biophotonics*, 2013, 6, 393.
- [5] J. Yoon, Y. J. Jo, M. H. Kim, K. Kim, S. Y. Lee, S. J. Kang and Y. K. Park, *Sci. Rep.*, 2017, 7, 6654.
- [6] L. Liu, M. E. Kandel, M. Rubessa, S. Schreiber, M. B. Wheeler and G. Popescu, *J. Biomed. Opt.*, 2018, 23, 025003.
- [7] P. Wang, R. Bista, R. Bhargava, R. E. Brand and Y. Liu, *Opt. Lett.*, 2010, 35, 2840.
- [8] R. K. Bista, S. Uttam, P. Wang, K. Staton, S. Choi, C. J. Bakkenist, D. J. Hartman, R. E. Brand and Y. Liu, *J. Biomed. Opt.*, 2011, 16, 070503.
- [9] P. Girshovitz and N. T. Shaked, *Opt. Express*, 2013, 21, 5701.
- [10] P. Girshovitz and N. T. Shaked, *Biomed. Opt. Express*, 2012, 3, 1757.
- [11] B. Rappaz, P. Marquet, E. Cuhe, Y. Emery, C. Depeursinge and P. J. Magistretti, *Opt. Express*, 2005, 13, 9361.
- [12] B. Rappaz, A. Barbul, Y. Emery, R. Korenstein, C. Depeursinge, P. J. Magistretti and P. Marquet, *Cytom. Part A*, 2008, 73A, 895.
- [13] M. R. Jafarfard, S. Moon, B. Tayebi and D. Y. Kim, *Opt. Lett.*, 2014, 39, 2908.
- [14] D. Boss, J. Kühn, P. Jourdain, C. Depeursinge, P. J. Magistretti and P. Marquet, *J. Biomed. Opt.*, 2013, 18, 036007.
- [15] B. Rappaz, F. Charrière, C. Depeursinge, P. J. Magistretti and P. Marquet, *Opt. Lett.*, 2008, 33, 744.
- [16] B. Kemper, S. Kosmeier, P. Langehanenberg, G. von Bally, I. Bredebusch, W. Domschke and J. Schnekenburger, *J. Biomed. Opt.*, 2007, 12, 054009.
- [17] S. Kosmeier, B. Kemper, P. Langehanenberg, I. Bredebusch, J. Schnekenburger, A. Bauwens and G. von Bally, in *Proc. SPIE 6991, Biophotonics: Photonic Solutions for Better Health Care*, Strasbourg, France, 2008, p. 699110.

- [18] M. Schürmann, J. Scholze, P. Müller, C. J. Chan, A. E. Ekpenyong, K. J. Chalut and J. Guck, *Method. Cell Biol.*, 2015, *125*, 143.
- [19] N. Lue, G. Popescu, T. Ikeda, R. R. Dasari, K. Badizadegan and M. S. Feld, *Opt. Lett.*, 2006, *31*, 2759.
- [20] L. Kastl, M. Isbach, D. Dirksen, J. Schnekenburger and B. Kemper, *Cytom. Part A*, 2017, *91*, 470.
- [21] P. Müller, M. Schürmann, S. Girardo, G. Cojoc and J. Guck, *Opt. Express*, 2018, *26*, 10729.
- [22] J. Min, B. Yao, V. Trendafilova, S. Ketelhut, L. Kastl, B. Greve and B. Kemper, *J. Biophotonics*, 2019, *12*, e201900085.
- [23] G. Dardikman, Y. N. Nygate, I. Barnea, N. A. Turko, G. Singh, B. Javidi and N. T. Shaked, *Biomed. Opt. Express*, 2018, *9*, 1177.
- [24] N. Cardenas, N. Ingle, L. Yu and S. Mohanty, in *Proc. SPIE 7904, Three-Dimensional and Multidimensional Microscopy: Image Acquisition and Processing XVIII*, San Francisco, California, United States, 2011, p. 790409.
- [25] M. Balberg, M. Levi, K. Kalinowski, I. Barnea, S. K. Mirsky and N. T. Shaked, *J. Biophotonics*, 2017, *10*, 1305.
- [26] C. L. Curl, C. J. Bellair, T. Harris, B. E. Allman, P. J. Harris, A. G. Stewart, A. Roberts, K. A. Nugent and L. M. D. Delbridge, *Cytom. Part A*, 2005, *65A*, 88.
- [27] A. Kus, M. Dudek, B. Kemper, M. Kujawinska and A. Vollmer, *J. Biomed. Opt.*, 2014, *19*, 046009.
- [28] M. Habaza, M. Kirschbaum, C. Guernth-Marschner, G. Dardikman, I. Barnea, R. Korenstein, C. Duschl and N. T. Shaked, *Adv. Sci.*, 2017, *4*, 1600205.
- [29] S. Chowdhury, W. J. Eldridge, A. Wax and J. Izatt, *Optica*, 2017, *4*, 537.
- [30] W. Choi, C. Fang-Yen, K. Badizadegan, S. Oh, N. Lue, R. R. Dasari and M. S. Feld, *Nat. Methods*, 2007, *4*, 717.

- [31] J. W. Su, W. C. Hsu, C. Y. Chou, C. H. Chang and K. Bin Sung, *J. Biophotonics*, 2013, 6, 416.
- [32] Y. Sung, W. Choi, C. Fang-Yen, K. Badizadegan, R. R. Dasari and M. S. Feld, *Opt. Express*, 2009, 17, 266.
- [33] Z. A. Steelman, W. J. Eldridge, J. B. Weintraub and A. Wax, *J. Biophotonics*, 2017, 10, 1714.
- [34] M. Schürmann, J. Scholze, P. Müller, J. Guck and C. J. Chan, *J. Biophotonics*, 2016, 9, 1068.
- [35] M. Habaza, B. Gilboa, Y. Roichman and N. T. Shaked, *Opt. Lett.*, 2015, 40, 1881.
- [36] M. Schürmann, G. Cojoc, S. Girardo, E. Ulbricht, J. Guck and P. Müller, *J. Biophotonics*, 2018, 11, e201700145.
- [37] A. Nakano, *Cell Struct. Funct.*, 2002, 27, 349.
- [38] J. Oreopoulos, R. Berman and M. Browne, *Method. Cell Biol.*, 2014, 123, 153.
- [39] S. Shapira, A. Shapira, D. Kazanov, G. Hevroni, S. Kraus and N. Arber, *Oncotarget*, 2017, 8, 38581.
- [40] D. Roitshtain, N. A. Turko, B. Javidi and N. T. Shaked, *Opt. Lett.*, 2016, 41, 2354.
- [41] P. Girshovitz and N. T. Shaked, *Opt. Lett.*, 2014, 39, 2262.
- [42] D. C. Ghiglia and M. D. Pritt, *Two-dimensional phase unwrapping: theory, algorithms, and software*, John Wiley and Sons, Inc., New York, 1998.
- [43] H. Satoh, L. M. D. Delbridge, L. A. Blatter and D. M. Bers, *Biophys. J.*, 1996, 70, 1494.
- [44] A. Kaur, L. Kaur and S. Gupta, *Int. J. Comput. Appl.*, 2012, 59, 32.
- [45] S. Gupta, L. Kaur, R. C. Chauhan and S. C. Saxena, *Digit. Signal Process.*, 2007, 17, 542.
- [46] M. Kumar, X. Quan, Y. Awatsuji, C. Cheng, M. Hasebe, Y. Tamada and O. Matoba, *J. Biomed. Opt.*, 2020, 25, 032010.

FIGURES

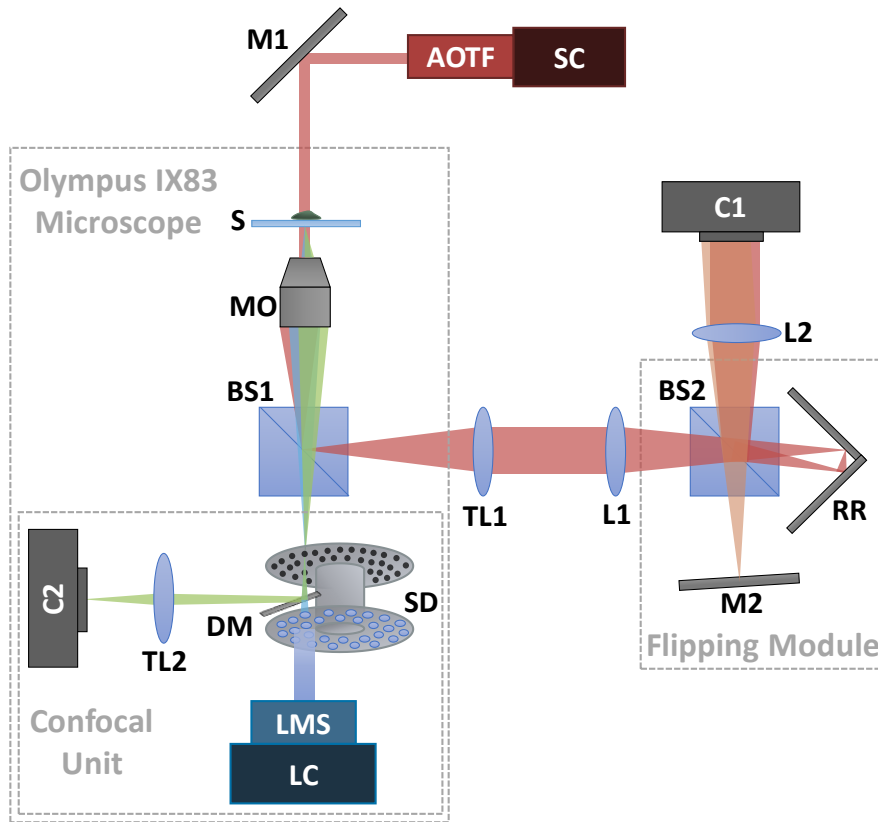


FIGURE 1. Scheme of the combined IPM and SDCM imaging system. The IPM beams appear in red; the fluorescent excitation beams appear in blue; the fluorescent emission beams appear in green. SC, supercontinuum laser source; AOTF, acousto-optic tunable filter; M1, M2, mirrors; S, sample; MO, microscope objective; BS1, BS2, beam splitters; TL1, TL2, tube lenses; L1, L2, lenses; RR, retro-reflector; C1, C2, digital cameras; LC, multi-line laser source; LMS, laser merge module; SD, spinning disk; DM, dichroic mirror.

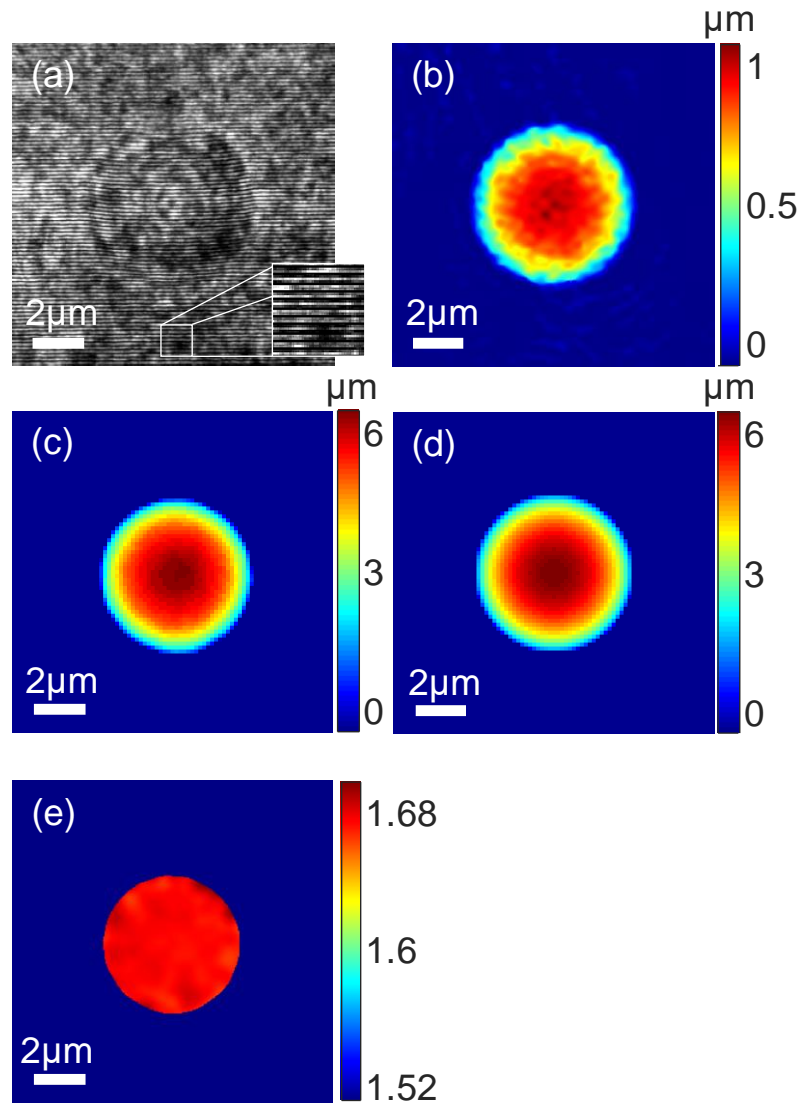


FIGURE 2. Representative images for 6- μm beads analysis. (a) Off-axis hologram. (b) OPD of the bead, as measured by IPM. (c) Fluorescence-confocal-based measured thickness profile of the bead. (d) Theoretical thickness of the bead assuming a perfect sphere. (e) Calculated RI map of the bead. In (b-d), the colorbars represent OPD or thickness values in μm . In (e), the colorbar represents RI values.

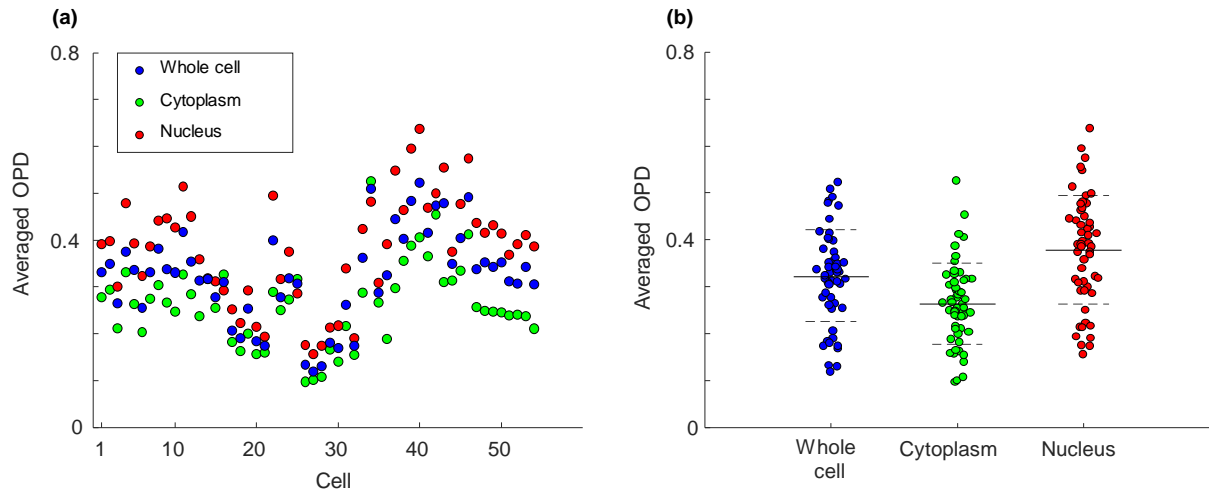


FIGURE 3. Averaged OPD values of the whole cell (blue), the cytoplasm (green) and the nucleus (red) locations, as indicated by 2D fluorescence microscopy: (a) for each cell and with the different organelles indicated, and (b) for each organelle but for groups of cells. In (b), the solid lines represent the group mean and the dashed lines represent the group STD.

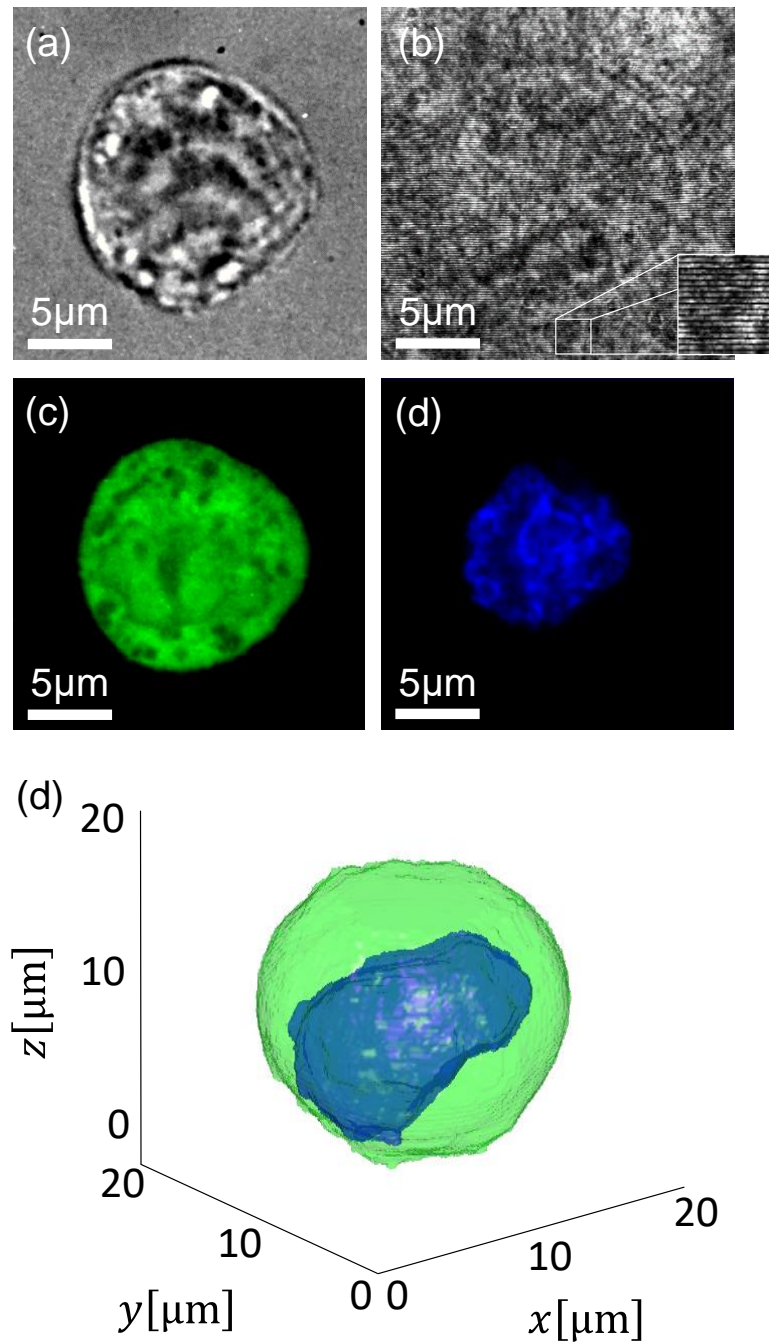


FIGURE 4. Representative images obtained by the combined IPM / SDCM imaging system for a HT29-GFP cancer cell in suspension. (a) BFM image. (b) Off-axis hologram. (c) Middle section of the confocal fluorescent signal of the whole cell. (d) Middle section of the confocal fluorescent signal of the nucleus. (e) Illustration of the 3D image reconstructed from the confocal fluorescent sections of the whole cell (green) and the nucleus (blue).

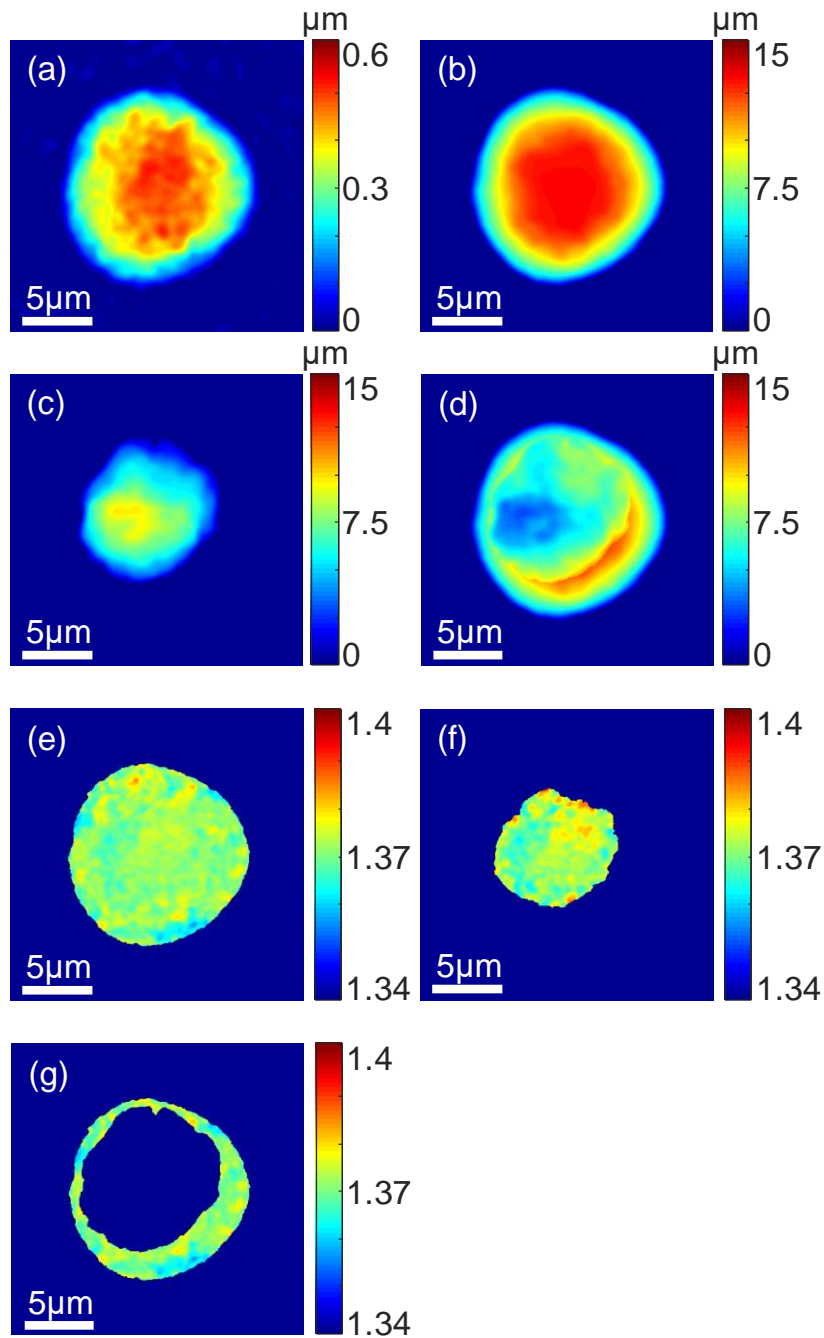


FIGURE 5. Processing stages of a representative HT29-GFP cell. (a) OPD profile of the entire cell. (b) Whole cell thickness, as obtained from the confocal fluorescent sections. (c) Nucleus thickness, as obtained from the confocal fluorescent sections. (d) Cytoplasm thickness, as obtained from the confocal fluorescent sections. (e) Whole cell integral RI. (f) Nucleus integral RI. (g) Cytoplasm integral RI. In (a-d), the colorbars represent OPD or thickness values in μm . In (e-g), the colorbars represent RI values.

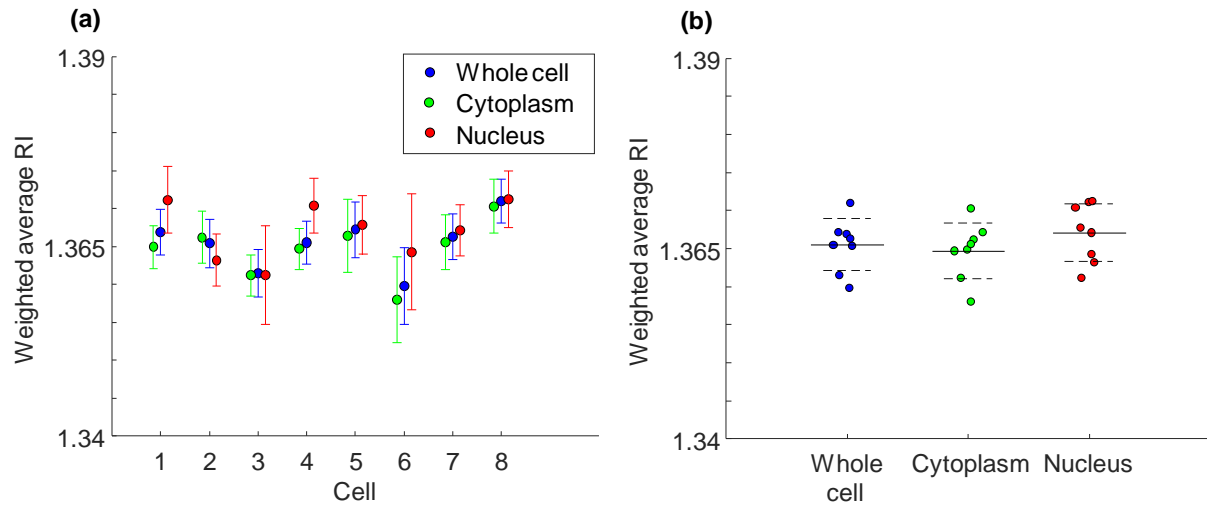


FIGURE 6. Weighted average RI values of the whole cell, the cytoplasm and the nucleus: (a) for each cell and with the different organelles indicated, and (b) for each organelle but for groups of cells. In (a) the error bars represent the STD, and in (b) the solid lines represent the group mean and dashed lines represent the group STD.

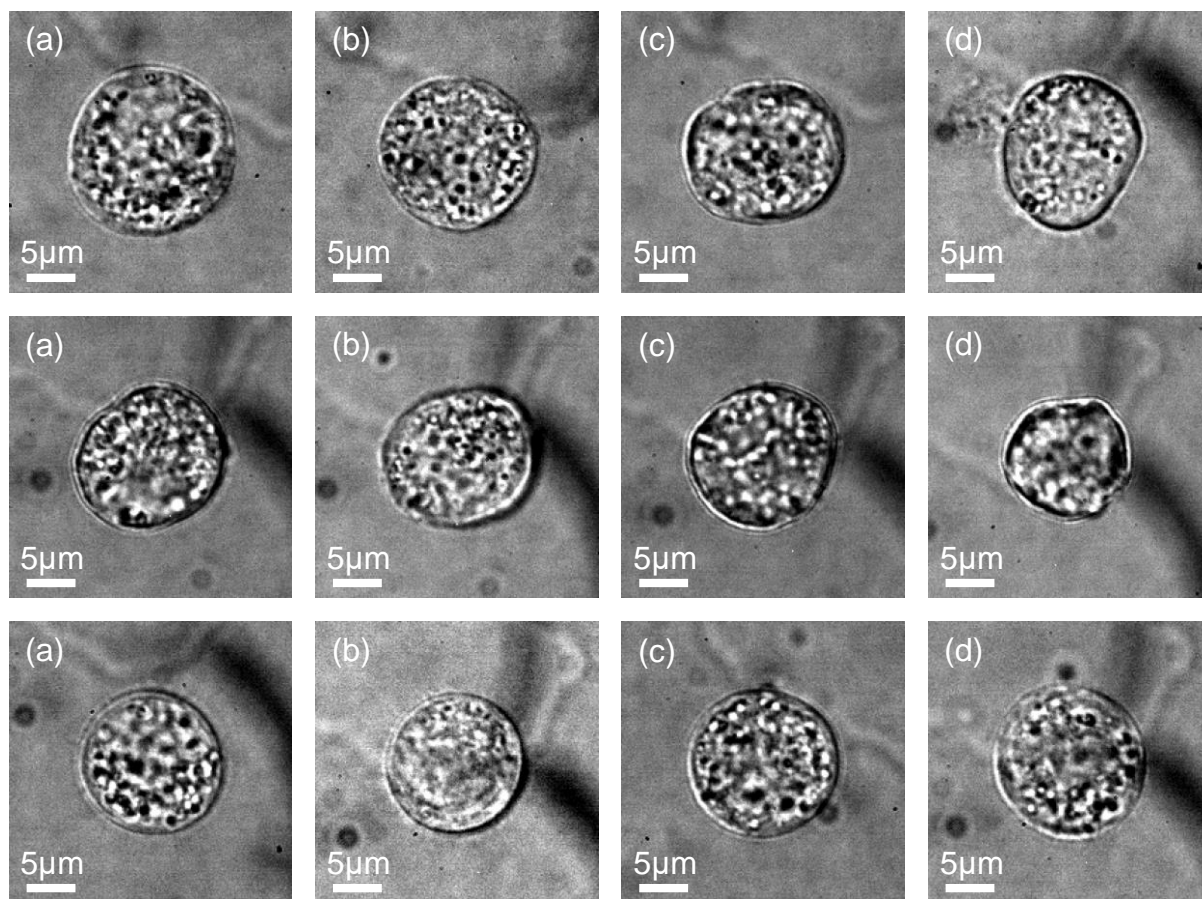


FIGURE 7. BFM images of the HT29-GFP cells, demonstrating the low RI differences of intracellular structures.

Graphical Abstract

We present a method for measuring the integral refractive index of cell organelles, integrating interferometric phase microscopy and rapid confocal fluorescence microscopy. From interferometric phase microscopy, we calculate the quantitative cell optical path difference, which is the product of the cell integral refractive index and physical thickness. From spinning-disk confocal fluorescence microscopy, we calculate the thickness of the entire cell and its nucleus. Finally, we find the integral refractive indices of the whole cell, cytoplasm, and nucleus for cancer cells.

